Neutron spectra in coincidence with γ rays from stopped π^- capture in ^{165}Ho

E. K. McIntyre, Jr., Y. K. Lee, T. J. Hallman, L. Madansky, and K. S. Kang
Department of Physics, The Johns Hopkins University, Baltimore, Maryland 21218

G. R. Mason
Department of Physics, University of Victoria, Victoria, British Columbia, Canada V8W 2Y2
(Received 9 December 1985)

Neutron spectra identified by final nuclear states have been measured for stopped π^- capture in ^{165}Ho. Neutron time of flight, with a resolution of 20% at 100 MeV, was collected in coincidence with the rotational γ-ray transitions in the even-even Dy isotopes. The inclusive spectrum was also measured in coincidence with pionic x rays, and agrees with previous singles measurements. The neutron spectra for individual final states show sharp cutoffs at characteristic energies, and, in some cases, the structure in the high energy component of the spectra is resolved. A Monte Carlo program based on the hybrid exciton model was developed, suitable for computing the inclusive and exclusive neutron spectra. The program gives a good fit to the measured inclusive spectrum. A different set of model parameters had to be used to reproduce the features of the spectra identified by the final nuclear states, and the fit was less satisfactory, indicating the need for an improvement in the preequilibrium approach which was not apparent in the past application to the inclusive spectra.

I. INTRODUCTION

The neutron spectra following nuclear capture of stopped π^- have been the subject of many experimental studies.[1-6] Recently, considerable progress has been made in the theoretical treatment of inclusive particle spectra in π^- capture.[7-13] A number of theories were successfully developed in the framework of cascade models[8-10] and other approaches with varying degrees of complexity.[11-13] Many of these theories, with diverse points of view, could reproduce the inclusive neutron spectra quite accurately. Further testing of the theory should come from examination of phenomena beyond the relatively simple shape of the inclusive spectra.

In the present experiment, the neutron spectra were measured in coincidence with discrete γ rays from the rotational ground state bands of the daughter nuclei. The target nucleus of ^{165}Ho was chosen because the range of almost stable isotopes of Dy, the daughter nuclides after π^- capture, is very wide and the collective rotational bands for most of these isotopes are well charted. The time-of-flight (TOF) spectra of neutrons were collected in coincidence with the discrete γ rays from the ground state band. The γ rays would then identify definite particle multiplicity and residual nuclear states. In particular, a set of five neutron spectra corresponding to final states in five even-even Dy nuclides was chosen for comparison with the predictions of a preequilibrium theory based on excitons.

The capture of a π^- by a single nucleon is inhibited. In the majority of cases the π^- is captured by a correlated nucleon pair. The rest mass of π^- is divided between the two resulting nucleons. The subsequent reaction is often described by preequilibrium nuclear processes until the nucleus reaches an equilibrium state. A large number of neutrons and γ rays are then emitted. The energetic component of emitted neutrons reflects the early stage of the reaction where each primary nucleon has undergone only a small number of nucleon-nucleon interactions, and during this stage, the "leading particles" can be described in the framework of a cascade model.

The exciton model[8] was used in the interpretation of the present experimental results. The hybrid version of the exciton model, which was a compromise between a complete cascade model and one allowing use of average behavior in an analytic form, was used here.[8,14] The emission cross section was given by the product of the intermediate state density and the branching ratio for emission. In this work, a major change was made in the usual treatment of the initial exciton state in order to represent the almost back-to-back kinematics of the primary nucleons. It will be shown below that with this change the hybrid exciton model reproduces the measured inclusive neutron spectrum to a high degree of precision without invoking further refinement such as nuclear density distribution, or using other than the usual set of model parameters. The hybrid exciton model was intended mainly to calculate the inclusive spectra analytically;[14] a new strategy was necessary in order to adapt the model to the calculation of exclusive neutron spectra. A Monte Carlo program was developed in this work which utilized the analytical approach of the hybrid model to compute the emission cross section and accomplished an important economy in record keeping of the cascades of collisions. Throughout this work, the effect of the finite depth of the nuclear potential well was considered to be a major factor[8,14] and a general approach to this task was formulated.

II. EXPERIMENTAL ARRANGEMENT

Energy of neutrons from π^- capture was determined by TOF measurements in coincidence with γ rays defining the nuclear final states. The TOF system, with 12 large scintillators for neutrons, is shown in Fig. 1. The time

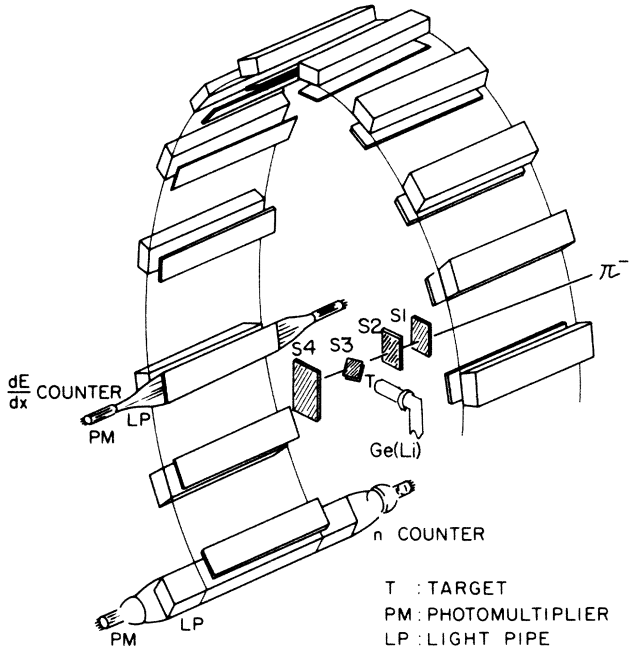

FIG. 1. The experimental arrangement of the detector system. The flight path from the target to the neutron counters is 1.5 m. Only one of the Ge(Li) detectors is shown.

zero was derived from the π^- stop signal in the thin scintillator (designated as $S3$), defining the fiducial volume of the target (T). One of the pair of γ-ray detectors is also shown next to the target in Fig. 1.

(a) *Beam, π^- telescope, and target.* The experiment was performed with a 90-MeV/c π^- beam from the $M13$ slow π channel at TRIUMF with 2% momentum resolution. The π^- stopping rate was 3×10^5/sec with appropriate polyethylene degrader, and the ratio of π:μ:e was estimated[15] to be 15:1:4. The $S3$ scintillator ($5\times5\times0.15$ cm^3) for timing a π^- stop was placed next to the target and was also included in the four-element telescope. The veto counter ($S4$) was used to eliminate events due to fast π^- not stopping in the target. The target was an isotopically pure ^{165}Ho, 600 mg/cm^2 thick, which was inclined to present 1000 mg/cm^2 to the beam.

(b) *γ-ray detectors.* Two large volume true coaxial Ge(Li) detectors were positioned at approximately 25 cm from the target for the measurement of photons. Each had a relative efficiency of 20% compared to a 7.5×7.5 cm^2 NaI crystal. The detectors provided 2.0 keV resolution at 1.33 MeV, although an onset of radiation damage was noticed towards the end of the experiment. The relative efficiency of the counters was determined by examination of spectra from ^{152}Eu and ^{182}Ta sources, and the absolute efficiencies were determined with a ^{137}Cs source. The correction for target self-absorption was large for γ rays below 200 keV, and a modification to the efficiency in this range was made to reproduce the correct pionic x-ray intensity.[5]

(c) *Neutron counters.* The 12 scintillators were placed with the long axis parallel to the beam at a distance of 1.5 m from the target, as shown in Fig. 1. The counters as a whole subtended a total of 3.7% of the 4π solid angle. The counters were separated by 20° in the azimuthal direction in order to reduce scattering from one counter into another. Each neutron counter consisted of a single piece of NE110 plastic scintillator, $7.5\times15\times62.5$ cm^3 in dimension, with a light pipe at each end designed to preferentially transmit "once reflected" light.[16] Constant fraction discriminators were used in all timing channels, and the signals from each pair of photomultipliers (Amprex XP2141) were processed in a mean-time mode. The timing resolution of the system was estimated from the width of the photon TOF peak. The full-width at half maximum (FWHM) was 0.9 ns, which led to an energy resolution of 5.6% at 10 MeV and 20% at 100 MeV. This is a conservative estimate of the resolution since heavy charged particles typically have better timing characteristics than photons.

The threshold for the neutron counters was set to be 1 MeV electron equivalent, with uncertainty within 20%. The threshold setting was used as an input to a Monte Carlo simulation of the detector efficiencies.[16] For the high energy neutrons of interest in this study, the efficiencies were essentially independent of the above quoted uncertainties in the determination of the threshold. The efficiencies for neutrons, based on Monte Carlo simulation, were modified so that each counter independently reproduced the 12-counter average of the neutron spectra coincident with the 6-5 pionic x-ray in Ho. The photon background in the neutron counters was effectively removed by the relatively high threshold setting and the TOF. The 6 mm thick dE/dx counters were used to veto charged

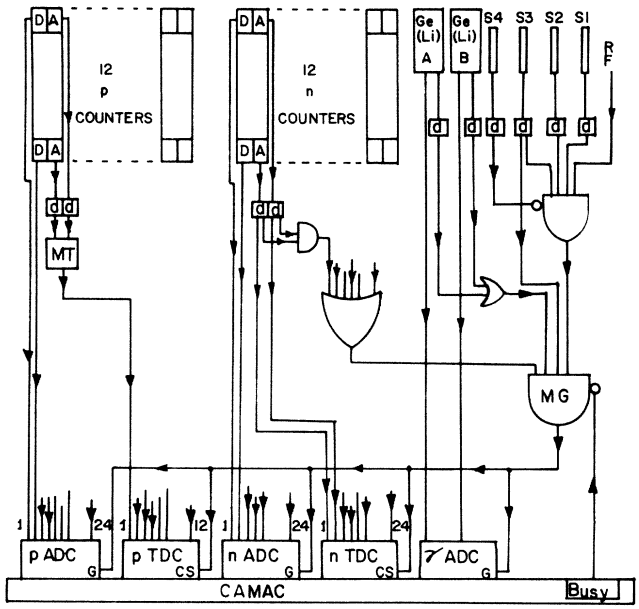

FIG. 2. A schematic of the electronics used to form the n-γ coincidences. Connections to discriminators and CAMAC modules are mostly omitted for clarity. The coincidence gate labeled MG is for the master gate indicating the triple n-π^--γ coincidences.

particle background.

(d) *Logic and electronics.* Data were collected in an event-by-event mode, with the event trigger defined by the triple coincidence of a π^- stop, a neutron, and a γ ray. As shown in Fig. 2, a π^- stop was indicated by the coincidence ($S1 \cdot S2 \cdot S3 \cdot \overline{S4} \cdot$rf) of the four counters in the telescope and the timing pulse (rf) derived from the radio-frequency source of the cyclotron. A γ ray was indicated by either of the two Ge(Li) counters. A neutron was indicated by a coincidence between the pair of photomultipliers for any of the 12 neutron counters. The triple n-π-γ coincidence, referred to in Fig. 2 as master gate (MG), was strobed by the timing scintillator $S3$ of the telescope to provide the start pulse for all the time-to-digital converter (TDC's). The anode pulses were used to provide the stop signal for individual TDC's. Pulse height information from Ge(Li) detectors and all the photomultipliers was collected through a CAMAC interface. The computer deadtime was less than 15%, for which the final neutron intensities were corrected.

III. ANALYSIS OF DATA

The n-γ coincidence data was analyzed in order to obtain the neutron TOF spectra identified by the final nuclear states. Clearly identifiable final nuclear states were members of the ground state bands in the even-even isotopes of Dy from $A=154$ to 162. Typically, spin states up to $12\hbar$ were identified in each isotope as in Fig. 3, but some higher spins were also detected. The details of the method of analysis and the estimate of the systematic errors are given below.

(a) *The extraction of neutron spectra from the* n-γ *coincidence data.* For each peak in the γ-ray spectra, three windows were selected: two side windows for the backgrounds on the lower- and the higher-energy sides and the third to represent the central region of the peak covering the FWHM of the peak. By including the FWHM region only for the off-line coincidence analysis, the signal-to-noise ratio was improved. Three neutron spectra, in coincidence with the γ rays in the respective windows, were then rendered as histograms. The background neutron spectra were then determined by interpolating the neutron spectra corresponding to the two side windows and subtracted from the spectra corresponding to the peak. Detailed fitting of the peak was not practical with the statistics of the coincidence data. An exception to the above procedure was the case of the poorly resolved peaks of the $6^+ \rightarrow 4^+$ transition in ^{154}Dy at 477.1 keV and the $10^+ \rightarrow 8^+$ transition in ^{158}Dy at 475.9 keV. In this case, the peak was divided into upper and lower halves. The other exception was the ^{160}Dy $8^+ \rightarrow 6^+$ transition which sat on the wing of the pionic 5-4 x-ray transition. A "flat background" estimate was made by extrapolating the average background in the higher-energy side background region, resulting in a probable underestimate of background.

(b) *Corrections to the neutron spectra.* The correction for the accidental coincidences in the TOF spectra was minor, but was carried out by the usual method of examining the range of negative delay in the TOF spectra. The

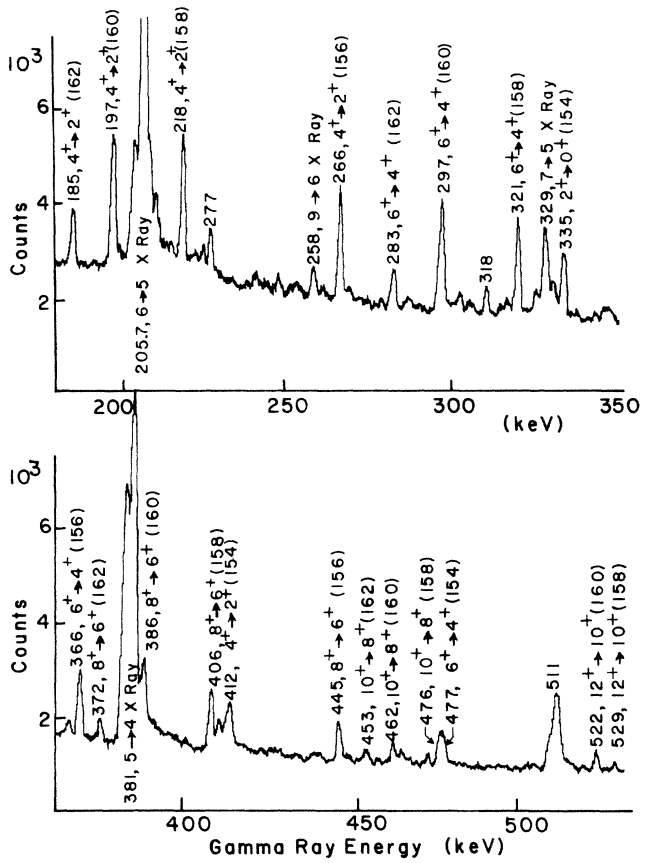

FIG. 3. The γ-ray spectrum from the π^- capture in ^{165}Ho. The rotational cascade γ rays of the Dy isotopes are identified by the spin-parity sequences of the transitions and by the nuclear mass number. The pionic x rays are also identified.

TOF spectra were then corrected for counter efficiencies. This procedure was repeated for each of the 12 neutron counters and then the results were combined into one TOF spectrum. Since only the area in the FWHM of the γ-ray peak was used in the coincidence analysis, the intensity was corrected to obtain the total intensity in the full peak by assuming the Gaussian shape of the peak. The data were also corrected for the computer deadtime and normalized by the total number of observed π^- stops.

(c) *Estimate of systematic errors.* The effect of the thickness of the counter ($\pm 2.5\%$ of the flight path) and the finite geometry of the target was estimated to be 5%. Systematic errors in the efficiency of the neutron counters included contributions from the Monte Carlo code for neutron efficiencies[16] estimated to be 5%; from the uncertainty in the threshold setting, which should be less than 10% for the energy range of interest in this experiment; from the final adjustment of the order of 10% of the efficiency discussed under the section on neutron counters. The efficiency of the Ge(Li) detectors was accurately determined by use of γ-ray sources and the effect of the target self-absorption of γ rays was small for the transition energies above 200 keV, with the combined uncertainty of 7% attributable to the γ-ray counters.

In obtaining the full peak intensity of a γ ray from the

FWHM data, the standard correction factor of 1.32 was used, assuming a Gaussian shape. Since the peaks were generally ten channels wide, an estimated error of two channels in the position of the half maximum points leads to ±6% error in this correction. Error was estimated more conservatively for those cases of poorly resolved γ-ray peaks. When the above estimates of errors are summed by quadrature, a systematic error of 18% is obtained for the intensity measurement.

IV. RESULTS

The results are presented here in the plots of the inclusive neutron spectrum and the neutron spectra in coincidence with particular γ-ray transitions from the ground state rotational bands. Salient spectral features of the neutron spectra including discrete structures near the maximum observed energy are discussed here, but the interpretation of the results is given in the next section in terms of the exciton model.

(a) *Inclusive spectrum.* The neutron spectrum in coincidence with the pionic 6-5 x ray in Ho, corrected for the known fluorescence yield[6] of 31% per stopped π^- in Ho, is shown in Fig. 4. Since the majority of the π^- captures take place from the $n=4$ atomic state and the 6-5 transition feeds the $n=4$ state, the neutron spectra in coincidence with the 6-5 x ray should be compared with the inclusive neutron spectrum reported from Scheweizerisches Institut für Nuklearforschung (SIN) (Ref. 17) also shown in Fig. 4. The Monte Carlo predictions for two different mean free path parameters to be discussed in the next section are also included in Fig. 4.

(b) *Spectra identified by neutron multiplicity.* The neutron spectra associated with the several ground state band transitions of a particular isotope can be summed to yield a single neutron spectrum associated with that isotope, as shown in Fig. 5 for the even-even Dy nuclei detected in this experiment. Each final state isotope corresponds to a different neutron multiplicity (M_n), with ^{162}Dy for $M_n=3$, up to ^{154}Dy for $M_n=11$. The kinematic limits for the neutron energy, based on the Q values of multiple neutron emission[18] and the pionic rest mass, are 57, 73, 89, 105, 120 MeV for $A=154$ to 162 (corresponding to $M_n=11,9,7,5,3$). Each spectrum in Fig. 5 extends to a characteristic limiting energy which is typically a few MeV less than the kinematic limit of the neutron energy. The spectra for the $A=156$, 158, and 160 cases show a peak near the maximum observed energy with an approximate width of 20 MeV. This is the first observation of such discrete features in the neutron spectra from π^- capture. These peaks may be due to the escape of one of the two primary neutrons with an energy approximately equal to the peak, leaving the nucleus in an excitation with a large probability of emitting M_n neutrons. These aspects are parametrized in a preequilibrium emission model and the model predictions are compared with the present measurements in the next section. The spectra for $A=154$ do not display any clear peaks. The absence of a peak suggests that both of the primary neutrons remain in the nucleus and that most of the π^- mass goes into the liberation of the 11 neutrons.

(c) *Spectra identified by individual nuclear states.* Examples of neutron spectra in coincidence with individual nuclear transitions are shown in Figs. 6 and 7. In these figures, neutron spectra in coincidence with the cascade γ rays from the rotational band are shown in sequence, in-

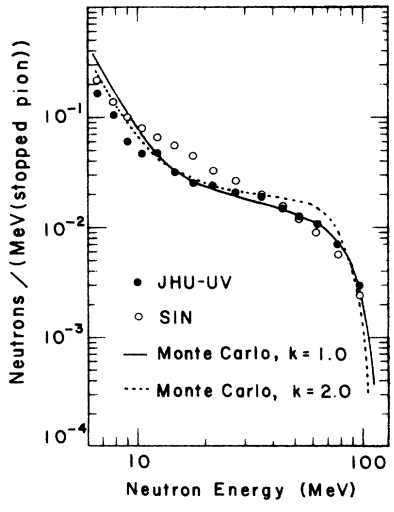

FIG. 4. Inclusive neutron spectrum from the π^- capture in ^{165}Ho from Ref. 17 (in open circles) compared to the neutron spectrum in coincidence with the 6-5 pionic x ray transition. The solid and dashed lines show the Monte Carlo results for $k=1.0$ and 2.0, respectively. Other parameters are $E_F=20$ MeV, $\sigma=33$ MeV, $\Theta=1.4$ MeV.

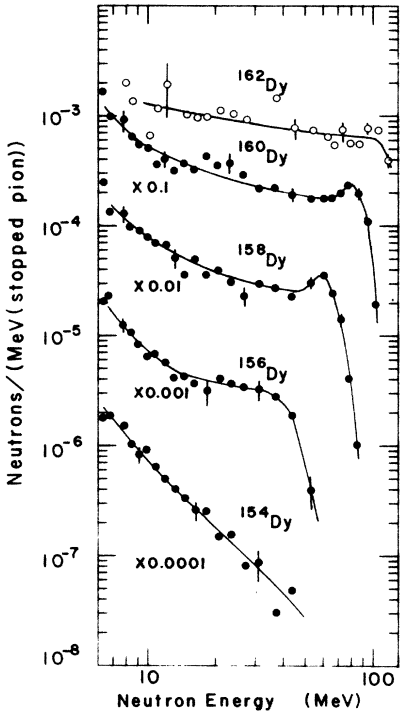

FIG. 5. Neutron spectra for reactions leading to the indicated final nuclides. The spectra represent the sum of the observed γ-ray intensities of ground state band for a particular isotope and do not necessarily represent the absolute cross section of production of the nuclides.

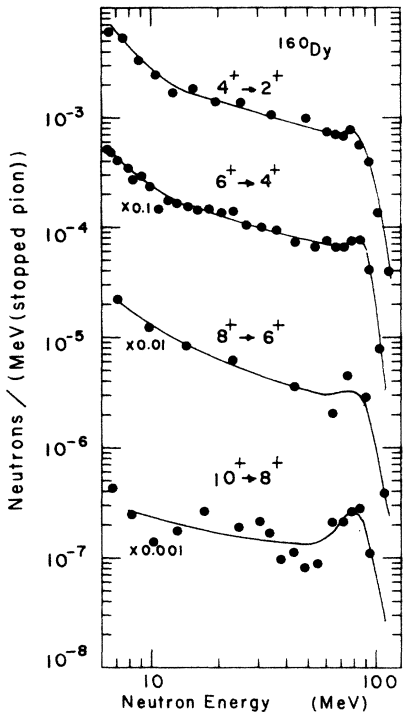

FIG. 6. Neutron spectra for reactions leading to specific spin states of ^{160}Dy. The errors are statistical.

cluding the highest member, the $10^+ \rightarrow 8^+$ transition. The contributions from the preceding γ-ray transitions are not subtracted from each spectrum. Some variation is seen in the relative importance of the thermal, preequilibrium, and discrete features, but the low statistics make such direct observations difficult. One method of observ-

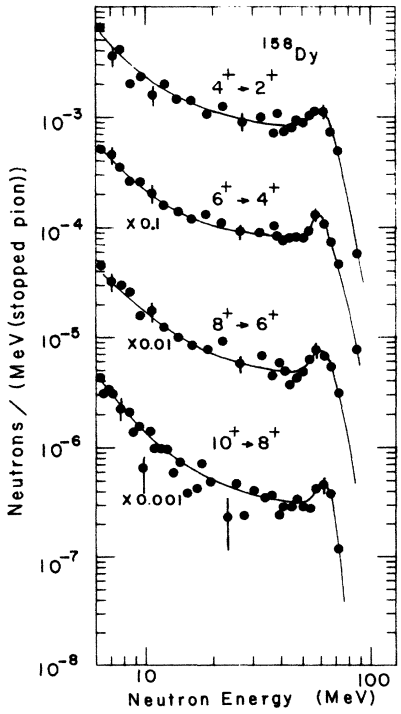

FIG. 7. Neutron spectra for reactions leading to specific spin states of ^{158}Dy. The errors are statistical.

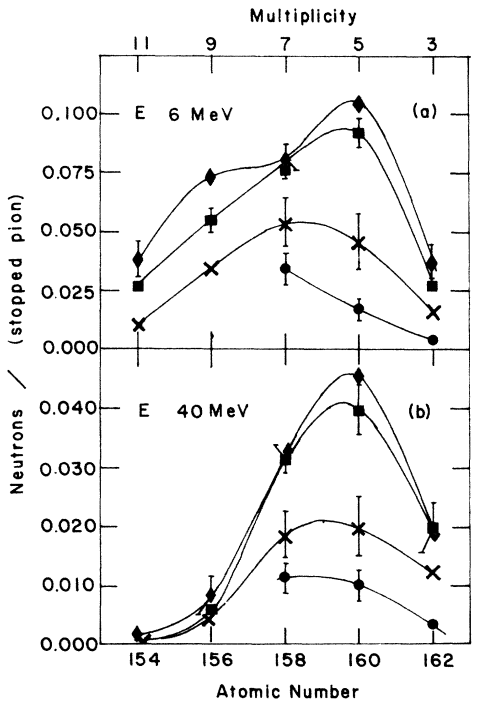

FIG. 8. (a) The intensity of neutrons with energy greater than 6 MeV for each of the ground state band transitions studied. The symbols are diamonds for $4^+ \rightarrow 2^+$, squares for $6^+ \rightarrow 4^+$, crosses for $8^+ \rightarrow 6^+$, and circles for $10^+ \rightarrow 8^+$ transitions, respectively. (b) As in (a) for neutron energy greater than 40 MeV.

ing trends in the data involves plotting the partially integrated intensities of the neutrons coincident with various γ-ray transitions. Figure 8(a) shows such a comparison for neutron energies greater than 6 MeV. The lines connect transitions between the same spin and parity states in different isotopes. It is noteworthy that the intensity peaks with ^{160}Dy for the top two curves, but shifts to lower atomic number for the bottom two curves. Similar conclusions can be drawn by examining the same type of plot, Fig. 8(b), for which the neutron energies are greater than 40 MeV. Further, the $4^+ \rightarrow 2^+$ and $6^+ \rightarrow 4^+$ transitions are almost identical for all isotopes, indicating that the direct side feeding to the 4^+ level is small. There is also a substantial drop in intensity of the $8^+ \rightarrow 6^+$ transition, suggesting that the dominant entry point to the ground state band cascade is the 6^+ state, at least for the $A = 158$, 160, and 162 cases.

V. EXCITON MODEL CALCULATION

In the hybrid exciton model,[14] the particle emission probability $P(\epsilon)$ for kinetic energy ϵ is given by the product of the probability of populating the continuum state $P_c(\epsilon, E_x)$ and the branching ratio $B(\epsilon)$:

$$P(\epsilon) = f P_c(\epsilon, E_x) B(\epsilon) \ . \quad (1)$$

Here, E_x is the energy of the exciton state, and f is the fraction for the correct type of nucleons. P_c is often called the intermediate state density in the literature of

preequilibrium analysis. In the present application, an essential change from the conventional exciton calculation was made in the treatment of the intermediate state density of the primary exciton state.

The hybrid exciton model was originally developed to calculate analytically the inclusive emission spectra $S(\epsilon)$:

$$S(\epsilon)=\sum_i f P_c^i(\epsilon,E_x)B(\epsilon)D_i \ , \tag{2}$$

where the sum is over the complete exciton cascade, and D_i is the survival factor of the fraction of the initial cross section surviving particle emission. In the current work, a new strategy was necessary for using the hybrid model to compute exclusive neutron spectra. This was accomplished by developing a Monte Carlo program in which each step of cascade was represented by $P(\epsilon)$ in expression (1), and the spectra were rendered as histograms separately for each final nuclear state or other dynamic variable. A detailed account of the present theoretical approach is given elsewhere.[19]

(a) *Treatment of the first exciton state.* The initial state after capture is conventionally treated as an exciton state with two particles and two holes that corresponds to the sudden excitation of two nucleons.[8] However, the states of the primary nucleons are more sharply defined than represented by a four-exciton state. In fact, the two nucleons almost equally share the π^- rest mass and depart in a back-to-back geometry.

In the present work, the pair of nucleons are assumed to occupy two independent shell states before the π^- capture takes place. The π^- rest mass is divided between the two nucleons according to a Gaussian distribution. The results are consistent with the observation of Gaussian spectra for the back-to-back emission of neutrons in light nuclei.[20] Nuclear well depth and the binding energy are also considered to play important roles. A careful examination of this situation[19] gives as the intermediate state density the following expression

$$P_c(\epsilon)=\begin{cases} 1/E_F & \text{for } E>E_F+E_B \ , \\ 1/(E-E_B) & \text{for } E<E_F+E_B \ , \end{cases} \tag{3}$$

where E_F is Fermi energy, E is excitation energy corresponding to the share of π^- rest mass for the nucleon, and E_B is neutron binding energy. It can be shown, using the correction for the finite phase space for hole states, that the above result is equivalent to treating the first exciton state as consisting of two independent exciton cascades, each with particle number 1, hole number 1, and an excitation energy corresponding to its share of the π^- rest mass.[19] This is a variation from our previous work[5] where two independent cascades beyond the primary exciton state were considered.

(b) *Effects of the finite phase space for the hole states.* The finite nuclear potential well depth limits the phase space of the hole states. This, in turn, has a profound effect on the energy range of the emitted particles. The importance of such an effect was recognized[10] and the correction for the first few exciton states has been reported before.[8] The following formula for the probability of populating the continuum state was derived[5,19,21] for the general case of any exciton states:

$$P_c(\epsilon,E_x)=f(n-1)\frac{\sum_{k=0}^{K}(-1)^k{}_hC_k(E_R-kE_F)^{n-2}}{\sum_{j=0}^{J}(-1)^j{}_hC_j(E_x-jE_F)^{n-1}} \ , \tag{4}$$

where E_x is the excitation energy of the exciton state, E_R is the excitation energy of the residual nucleus after emission, E_F is the Fermi energy; f is the fraction for the correct type of nucleons (neutron in this case), h is the hole number, K is the largest integer $\leq E_R/E_F$ not exceeding h in the residual nucleus, and J is the largest integer $\leq E_x/E_F$ not exceeding h in the initial nucleus.

(c) *Branching ratio.* The internal transition rate is calculated by use of the mean free path, and the emission rate is calculated by use of cross section of the inverse reaction (particle capture rate).[14] Following the parametric formulation,[8,22] the branching ratio used in this work is

$$R=\frac{\sigma_x\epsilon/g_x}{\sigma_x\epsilon/g_x+[1890(\epsilon+E_B)-8(\epsilon+E_B)^2]/k} \ , \tag{5}$$

where σ_x is the inverse cross section and k is a parameter defining the transition probability to the next higher exciton state by the expression[14]

$$\lambda_{n+2}(\epsilon)=[1.4\times10^{21}(\epsilon+E_B) -6.0\times10^{18}(\epsilon+E_B)^2]/k \ \text{sec}^{-1} \ .$$

In the energy range of interest $k=1$ corresponds to the mean free path of 3–4 fm.

(d) *Monte Carlo procedure.* At the initiation of the cascade, the mass of π^- is divided between two primary nucleons according to a Gaussian energy distribution with a width parameter σ. After the share of energy for each nucleon is picked, the kinetic energy of the nucleon is randomized according to the applicable case in expression (3). The branching ratio in expression (5) is used to compute any emission of the primary neutrons. For particles surviving from the previous exciton state, the total cross section of emission from the next exciton state is computed by integrating expression (1) over the allowed kinetic energy. Based on this cross section, the Monte Carlo program either randomizes the emission spectra according to expression (1) or continues to the next stage of cascade after incrementing particle and hole numbers by one. The factor f in expression (1) is adjusted by assigning one-half of the increment in particle number to neutrons, and the other half to protons. This process is repeated until the exciton state with $n=16$ is reached.

In the current work, the Monte Carlo program does not trace the sequential emission of thermal neutrons, but computes the multiplicity distribution of thermal neutrons based on the residual energy at the end of the exciton cascade, using the expression given by Lifshitz *et al.*[22] The spectra for thermal neutrons for nuclear temperature Θ is then added to the fast neutron spectra with intensity adjusted according to the multiplicity.

(e) *Comparison with experiments.* The inclusive neutron spectrum is computed with the parameters which were used in other exciton calculations to fit experimental data ($E_F=20$ MeV, $\Theta=1.4$ MeV, $k=1.0$).[5,8,14] The Gauss-

ian width σ for the division of π^- rest mass was chosen to be 33 MeV, corresponding to the situation discussed in Machner.[13] The results have already been discussed in connection with the experimental spectra in Fig. 4. A departure ($k=2.0$) from the values widely used in exciton calculations[14] gives the less satisfactory fit shown by the dotted line in Fig. 4, but this value gives the best visual fit to the neutron spectra in coincidence with the γ rays, which will be discussed later.

The relative importance of the ejectiles from the primary exciton state is shown in Fig. 9. Recently, the fast component of the inclusive neutron spectra was computed solely on the basis of the unhindered emission of one of the primary nucleons.[3,11] An examination of the spectra in Figs. 4 and 9 shows that the inclusive spectrum can be satisfactorily reproduced without overestimating the role of the escaping primary nucleon.

No attempt has been made so far to predict the population of individual spin-parity states in the final nuclei. The main prediction of the current calculation concerns the neutron spectra corresponding to definite final nuclides or, equivalently, the neutron multiplicities. On the other hand, the experimental results are always in coincidence with a transition involving individual spin-parity states so that an adjustment is necessary for comparison with the model predictions.

When the measured γ rays are summed for each nuclide as in Fig. 5, the intensity does not necessarily represent the correct population of the final nuclides since a substantial number of γ rays are not accounted for. A more serious problem caused by summing γ rays is the chance of double counting the population due to cascading γ rays. However, an inspection of Fig. 8 indicates that the intensities of transitions $4^+\rightarrow 2^+$ and $6^+\rightarrow 4^+$ are in the majority of cases equal within 30%, indicating that 6^+ state is a major entry point into the ground state rotational band. Therefore, in the current work, the Monte Carlo results for different multiplicities are compared to the neutron spectra in coincidence with the $4^+\rightarrow 2^+$ transitions in even-even final nuclides as shown in Fig. 10. The population of the odd spin states is assumed to be as probable as that of even spin states[5] so that the $4^+\rightarrow 2^+$ transitions represent only one-half of the picture. It is also assumed that roughly one-third of the cascade entered the ground state rotational band below 4^+ states. These assumptions are reasonable, but they can also be viewed as a Monte Carlo adjustment giving the best fit of absolute intensities for neutron multiplicities 7 and 9 in Fig. 10. Major features of the five spectra are reproduced by the Monte Carlo results, e.g, the cutoff behavior at characteristic energies, indication of broad peaks near the cutoff, and the filling in of the intermediate region. It was noticed that the distribution of absolute cross section among the five spectra was not sensitively affected by the variation of the Gaussian width from 18 to 40 MeV and the variation of Fermi energy from 18 to 25 MeV. The overestimate of the $M_n=11$ spectra could be caused by the overestimation of thermal neutrons as evidenced in the inclusive spectrum of Fig. 4. The large mean free path parameter, $k=2$, for the best fit in Fig. 10 could be related to the similar observation of the parameter larger than predicted either on the basis of imaginary optical potential or the Thomas-Fermi model,[23] or it may be due to the inadequacy of the formulas[22] used to calculate the thermal neutron multiplicity.

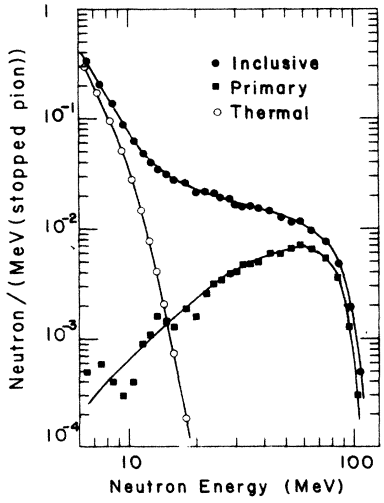

FIG. 9. Monte Carlo results for inclusive neutron spectrum from π^- capture in ^{165}Ho. Contribution from the primary nucleon emission spectrum and the thermal spectrum are also shown. $E_F=20$ MeV, $\sigma=33$ MeV, $\Theta=1.4$ MeV, $k=1.0$.

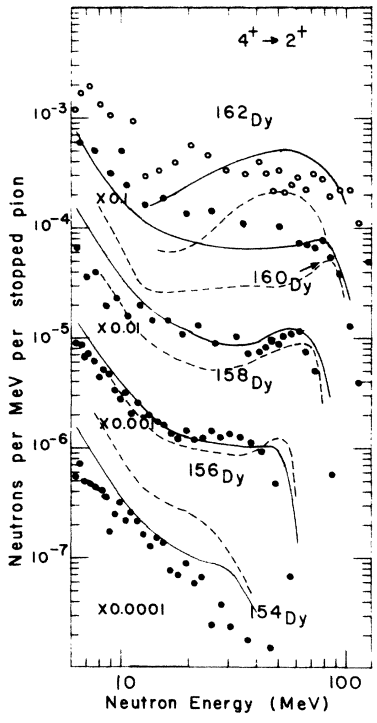

FIG. 10. Neutron spectra from the π^- capture in ^{165}Ho measured in coincidence with the $4^+\rightarrow 2^+\gamma$-ray transitions. The solid curves are the results of Monte Carlo with $E_F=20$ MeV, $\sigma=25$ MeV, $\Theta=1.4$ MeV, $k=2.0$; and the dashed curves are with $k=1.0$.

VI. CONCLUSION

Neutron spectra correlated to discrete γ rays from the final nuclear states show a sharp cutoff at characteristic energies, and in some cases, exhibit resolved structure in the high energy component, a feature not seen in the inclusive spectrum. In particular, the neutron spectra corresponding to final states in five even-even Dy nuclides were chosen for comparison with the predictions of a preequilibrium theory based on the hybrid exciton model. The usual treatment of the first exciton state by a two-particle and two-hole state was discarded in favor of a description of the back-to-back kinematics of the primary pair of nucleons which share the π^- rest mass. The analytical approach to the cascades, inherent to the hybrid exciton model, was modified in a Monte Carlo program suitable for constructing histograms of exclusive spectra. When a set of generally accepted model parameters was used, and the effects of the finite phase space for hole states were taken into account, the model reproduced the inclusive neutron spectra with high precision. When the model was put to the task of reproducing multiple spectra from this experiment, the mean free path parameter had to be increased considerably, which resulted in an overestimate of the energetic component in the inclusive spectrum. The computation of the relative importance of the ejectiles from the primary state showed that its importance in forming the fast neutron spectra was overestimated in the past.[11,13] The data on the exclusive spectra provide the necessary constraints for improving the models which successfully reproduce inclusive spectra.

ACKNOWLEDGMENTS

The authors wish to acknowledge the participation by A. J. Caffrey, the excellent support by the TRIUMF staff, and the use of computation facilities of the High Energy Physics Group at Johns Hopkins University. This work was partially supported by a contract with the U.S. Department of Energy.

[1]V. S. Buttsev *et al.*, Fiz. Elem. Chastits At. Yadra **11**, 900 (1980) [Sov. J. Part. Nucl. **11**, No. 4, 358 (1980)].
[2]V. J. Orth *et al.*, Phys. Rev. C **21**, 2524 (1980).
[3]H. P. Isaak *et al.*, Nucl. Phys. **A392**, 368 (1983).
[4]J. Julien *et al.*, Phys. Rev. C **23**, 448 (1981).
[5]A. Shor *et al.*, Nucl. Phys. **A420**, 553 (1984).
[6]R. Levin *et al.*, Phys. Lett. **114B**, 427 (1982).
[7]R. P. Redwine, Nucl. Phys. **A434**, 239c (1985).
[8]M. Blann, Phys. Rev. C **28**, 1648 (1983).
[9]A. S. Iljinov, V. I. Nazaruk, and S. E. Chigrinov, Nucl. Phys. **A268**, 513 (1976).
[10]E. Gadioli and E. Gadioli Erba, Nucl. Phys. **A256**, 414 (1976).
[11]N. C. Mukhopadhyay, Nucl. Phys. **A319**, 448 (1979).
[12]H. C. Chiang and J. Hüfner, Nucl. Phys. **A352**, 442 (1981).
[13]H. Machner, Nucl. Phys. **A395**, 457 (1983).
[14]M. Blann, Annu. Rev. Nucl. Sci. **25**, 428 (1975).
[15]C. Oram *et al.*, Nucl. Instrum. Methods **179**, 95 (1981).
[16]M. Elfield *et al.*, Nucl. Instrum. Methods **100**, 237 (1972).
[17]W. Dey *et al.*, Helv. Phys. Acta **49**, 778 (1976).
[18]*Table of Isotopes*, 7th ed., edited by C. M. Lederer and V. S. Shirley (Wiley, New York, 1978).
[19]Y. K. Lee, Phys. Rev. C **33**, 1707 (1986).
[20]B. Bassalleck *et al.*, Phys. Rev. C **19**, 1893 (1979).
[21]R. Levin, Ph.D. thesis, The Johns Hopkins University, 1983.
[22]M. Lifshitz and P. Singer, Phys. Rev. C **22**, 2135 (1980).
[23]E. Gadioli, E. Gadioli Erba, and J. J. Hogan, Phys. Rev. C **16**, 1404 (1977).